An experimental investigation of transitions between the metastable states of superconducting weak-link rings containing a niobium point contact

1991 J. Phys.: Condens. Matter 3 6079

(http://iopscience.iop.org/0953-8984/3/32/014)

J. Phys.: Condens. Matter 3 (1991) 6079–6092. Printed in the UK

An experimental investigation of transitions between the metastable states of superconducting weak-link rings containing a niobium point contact

M N Keene, C E Gough and A I M Rae
Superconductivity Research Group, School of Physics and Space Research, University of Birmingham, Edgbaston, Birmingham B15 2TT, UK

Received 14 February 1991

Abstract. Careful measurements have been made of the critical currents of a number of superconducting weak links formed using niobium point contacts. Values for these critical currents as functions of temperature have been derived both from magnetization curves obtained when the links were included in a structure with a two-hole SQUID geometry and from current–voltage measurements. The data were corrected for the effects of thermal activation. Discrepancies between the results and theoretical predictions were attributed to non-sinusoidal current–phase relationships; magnetization measurements were performed on very weak links which produced direct evidence for this effect. The standard theoretical model was modified to include a second-harmonic term in the current–phase relationship and the resulting predictions agreed well with the experimental results. No evidence was obtained for macroscopic quantum tunnelling in our devices, which is consistent with the prediction that this effect should be suppressed by the electromagnetic properties of the superconducting structure surrounding the point contact.

1. Introduction

Superconducting rings containing one or more weak links underlie the operation of all SQUID (superconducting quantum interference device) systems. Before the development of commercially reliable thin-film structures, niobium point contacts were often used as the weak link, the naturally occurring oxide layer on the surface forming the thin insulator between the regions of contact.

Such structures were also used by Prance *et al* [1], den Boer and de Bruyn Ouboter [2] and de Bruyn Ouboter [3] to investigate the possible occurrence of macroscopic quantum tunnelling (MQT) between the metastable flux states of weak-link rings. Transitions between these states can occur either by thermal excitation of the system over the potential barrier provided by the weak link, which is of order $E_J = \Phi_0 i_c/2\pi$ (where $\Phi_0 = h/2e$ is the flux quantum and i_c the critical current associated with the weak link), or by quantum mechanical tunnelling through the barrier. For MQT to be observed either the capacitance of the link must be extremely small or the temperature must be extremely low so that tunnelling dominates the effects of thermal excitation. Some of the above experimental work claims to have observed MQT at temperatures above 1 K, implying an effective capacitance of the weak-link structure of less than about 10^{-15} F, but, unfortunately, there is no way of providing an independent measurement of the actual

0953-8984/91/326079 + 14 $03.50

capacitance in these measurements. More recently, others [4, 5] have used thin-film structures with a more precisely defined capacitance and have been able to demonstrate a transition from thermal activation at high temperatures to MQT at low temperatures.

The earlier point-contact measurements remain problematical as, although it may be true that the capacitance between the actual contact area of the point can be of the order of 10^{-15} F, this capacitance appears in parallel with the capacitance of the point itself and the surrounding structure. The latter can be estimated to be of order 10^{-12} F, which would completely rule out the possibility of observing MQT at the temperatures claimed. Indeed, a detailed analysis of MQT in a point-contact geometry [6] confirms that, for low frequencies, it is the total capacitance in parallel with the point that determines the tunnelling probability and that at high frequencies the characteristic impedance of the SQUID structure seen by the point serves to introduce damping, which substantially reduces the tunnelling probability. In either case the probability of MQT is reduced to the point where it should not have been observable in the regime where the point-contact experiments were conducted. More recently, calculations have shown that the electromagnetic environment should act in a similar manner to suppress the 'Coulomb blockade' in single-electron tunnelling [7].

The present work was carried out with the aim of reinvestigating transitions in point-contact structures. As far as possible, all the relevant parameters of the point-contact structure have been determined independently from the observed flux transition probabilities. This has included independent measurements of the DC electrical and magnetic characteristics, the current–phase relationships of the various point contacts studied and an absolute measurement of the inductance of the weak-link ring. Our measurements extend over the temperature range 1.2 to 9 K and were undertaken in a well screened environment to eliminate electromagnetic noise, which could otherwise simulate the effect of MQT.

No evidence was found for MQT in any of the point contacts investigated and all the measurements could be described by thermal activation. Nevertheless, significant deviations from the assumptions implicit in the simple models generally used to describe MQT in weak-link structures were observed. In particular, after taking into account thermal activation [8], significant deviations in the temperature dependence of the intrinsic critical current compared from that predicted by Ambegaokar and Baratoff [9] were noted. Furthermore, significant deviations from a sinusoidal current–phase relationship were observed, which strongly influences the transition probabilities near the critical state. Failure to take such deviations into account could lead to an incorrect interpretation of the temperature dependence of the transition probability meaurements.

2. Theory

The energy of a superconducting ring interrupted by a weak link may be expressed as

$$E(\phi, \phi_x) = (\phi - \phi_x)^2/2L - \varepsilon_j(\phi) \tag{1}$$

where ϕ_x and ϕ are the applied flux and the total flux (hereinafter referred to as the

'internal flux') in the ring, respectively, L is the inductance of the ring and ε_j is the flux-dependent junction energy. The relationship between ϕ and ϕ_x at equilibrium is obtained by minimizing E to give

$$\phi_x = \phi + L\,\partial\varepsilon_j(\phi)/\partial\phi. \tag{2}$$

For an ideal Josephson junction where the Cooper pairs tunnel one at a time, the junction energy is given by

$$\varepsilon_j(\phi) = (\Phi_0/2\pi)I_c\cos(2\pi\phi/\Phi_0) \tag{3}$$

where I_c is the critical current of the junction and Φ_0 is the magnetic flux quantum. The equilibrium relation between ϕ and ϕ_x is now

$$\phi_x = \phi + (\Phi_0/2\pi)\beta\sin(2\pi\phi/\phi_0) \tag{4}$$

where

$$\beta = 2\pi LI_c/\Phi_0. \tag{5}$$

The properties of the relationship (4) between ϕ and ϕ_x depend on the value of β. If β is greater than one, it is multivalued and displays hysteresis when ϕ_x is cycled through a flux quantum as shown in figure 1(*a*), whereas, if β is less than one, it is non-hysteretic (figure 1(*b*)). For both curves the slope at the origin is $1/(1+\beta)$.

The relationships neglect both the effects of thermal activation at finite temperatures and possible macroscopic tunnelling. At a finite temperature, thermal activation causes early jumps, as described by Kurkijarvi [10], with a distribution in jump probabilities dependent on both temperature and the junction parameters. At sufficiently high temperatures, the jump probability can be so high that many jumps backwards and forwards occur within the time of any single measurement, so that even when β is greater than one, the curves appear non-hysteretic, with a thermally averaged ϕ given by

$$\langle\phi\rangle = \int_{-\infty}^{\infty}\phi\exp[-E(\phi,\phi_x)/kT]\,\mathrm{d}\phi \Big/ \int_{-\infty}^{\infty}\exp[-E(\phi,\phi_x)/kT]\,\mathrm{d}\phi \tag{6}$$

where $E(\phi,\phi_x)$ is given in (1) and becomes, in the case of the sinusoidal relationship (4)

$$E(\phi,\phi_x) = I_c\left[\frac{\pi}{\Phi_0}\frac{(\phi-\phi_x)^2}{\beta} - \frac{\Phi_0}{2\pi}\cos\left(\frac{2\pi\phi}{\Phi_0}\right)\right]. \tag{7}$$

The effects of thermal activation are illustrated for hysteretic and non-hysteretic junctions in figures 1(*a*) and 1(*b*). By fitting the experimentally determined magnetization curves (i.e. $\langle\phi\rangle$ plotted against ϕ_x) to equation (6) it is possible to derive values for both β and I_c, which are related through the ring inductance L. In practice, as we shall show later, we also determine the inductance in a separate measurement, enabling us to make a critical comparison with theoretical predictions. Any discrepancies imply departures from the model used, such as the neglect of MQT and the assumed sinusoidal current–phase relationship.

The effect of MQT on the magnetic behaviour of the weak-link rings would be to cause early transitions between the metastable states even at absolute zero. Transitions would generally occur before the applied flux reached the critical value by an amount that would depend on the effective capacitance of the macroscopic system and the detailed shape of the current–phase relationship near criticality. The influence of MQT would

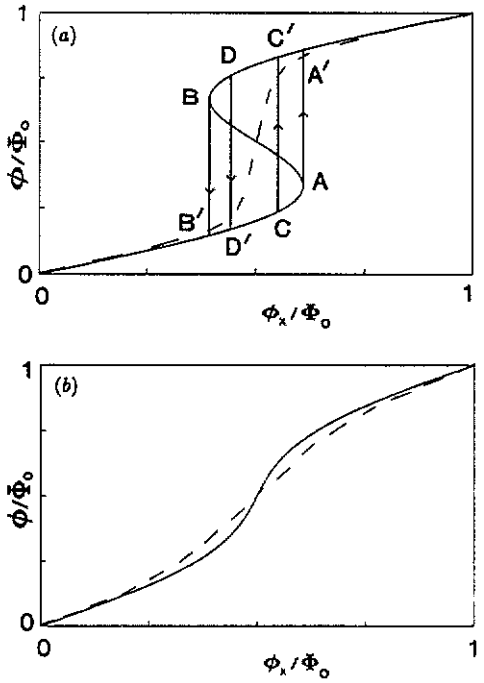

Figure 1. The continuous curves represent the theoretical dependence (4) of the total flux ϕ on the externally applied flux ϕ_x for two values of β. In (*a*), $\beta > 1$ and when ϕ_x is cycled between zero and ϕ_0, hysteretic behaviour following the paths AA′ and BB′ is expected at $T = 0$; at somewhat higher temperatures the paths CC′ and DD′ are followed and at higher temperature still the hysteresis becomes unobservable and the thermally averaged path indicated by the broken line is observed. In (*b*), $\beta < 1$ and the theoretical curve is non-hysteretic (full curve); at higher temperatures the thermally averaged behaviour is indicated by the broken curve.

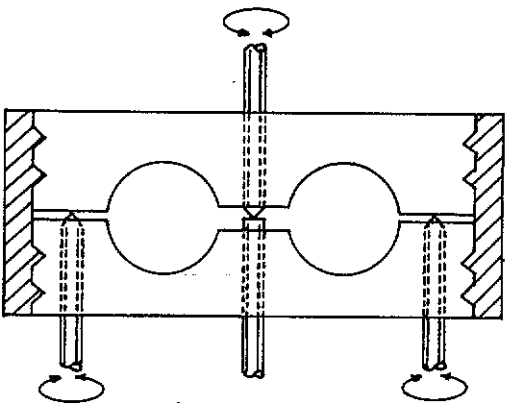

Figure 2. The experimental weak-link structure.

therefore be approximately equivalent to that of transitions at a temperature T^*, which would always be greater than the actual temperature of the system and would depend on the junction strength, the sinusoidal behaviour and the effective capacitance.

Our experiments were designed so that the ring could be broken to allow direct measurement of the I/V characteristics of the point contact used as the weak link in the magnetic measurements. In determining I_c from such measurements it is again necessary to account for the effect of early transitions caused by thermal excitation (or indeed MQT if this was significant). In particular, it is important to recognize that the measured values, $I_c(T)^*$, will be reduced by thermal excitation below the intrinsic values $I_c(T)$, used in the above analysis. The influence of thermal activation on the current–voltage characteristics was first discussed by Ivanchenko and Zil'berman [11] and more fully by Ambegaokar and Halperin [12]. One of us [8] has recently shown that, to a good approximation, $I_c(T)^*$ can be written as

$$I_c(T)^* = I_c(T)\left[1 - \left(\frac{kT\ln(I_c(0)R/V_{min})}{0.3I_c(T)\Phi_0}\right)^{2/3}\right] \quad (8)$$

where R is the normal-state resistance of the junction and V_{min} is the first detectable voltage used to define $I_c(T)^*$. Knowledge of the relevant parameters therefore enables measurements of $I_c(T)$ to be determined from the experimentally determined critical current $I_c(T)^*$.

3. Experimental

The weak-link structure investigated in these measurements is shown schematically in figure 2. It consists of two niobium blocks between a thin Mylar layer was clamped using insulated brass screws and Stycast end castings to provide additional structural rigidity. The point contact used as the weak link in these experiments was formed between the two inner 12 Ba niobium screws, one of which had a flat end to form the anvil and the other a carefully sharpened point. There was a spacing between two niobium blocks of 0.8 mm to enable the point contact to be positioned a few microns above the anvil prior to adjustment at low temperatures in the experiment itself. The outer two 12 BA niobium screws could be left open so that the current–voltage characteristics of the central point contact could be measured, or screwed hard down to complete the external superconducting circuits in a two-hole SQUID geometry. All three screws in the top surface of the niobium block could be adjusted mechanically from outside the cryostat using very fine micrometer drives. Subsequent mechanical isolation of the screws from their external drives minimized vibrational and electrical coupling problems.

The Nb points were sharpened to a tip of about 1 μm diameter by mechanical grinding. They were oxidized in air at room temperature for 24 hours and stored in a dry helium atmosphere before mounting. The anvil was similarly treated.

External flux was applied by a copper coil placed in one of the holes with the superconducting primary of a DC flux transformer connected to an external radio frequency SQUID in the second to measure the induced flux. The superconducting DC flux transformer was weakly coupled to the external measuring SQUID and also incorporated a normal metal resistive shunt to act as a low-pass filter, minimizing the possibility of spurious transitions induced from the external SQUID.

The niobium block was surrounded by two concentric superconducting shields inside a vacuum container surrounded by liquid helium. The temperature of the block could be varied between 1.2 K and 10 K by heaters and thermometers mounted outside the superconducting shields and strongly coupled thermally to the block via copper heat links. All the electrical leads to the niobium block were carefully filtered and also included 50 dB attenuation to room temperature to minimize radio frequency interference from external sources. The glass cryostat containing the experiment was surrounded by two Faraday cages and a mu-metal cylinder. The whole apparatus was placed inside a closed copper box, which was itself surrounded by soft-iron sheets for further magnetic screening. The SQUID and electronics controlling the temperature were powered by batteries inside the box, with analogue links providing communication with the outside of the box for control and measurement. Measurements were recorded digitally on a well screened microcomputer placed 5 m from the apparatus, with heavily filtered lines to the optical analogue receivers. By taking such extensive precautions, we believe we have effectively eliminated all sources of external interference.

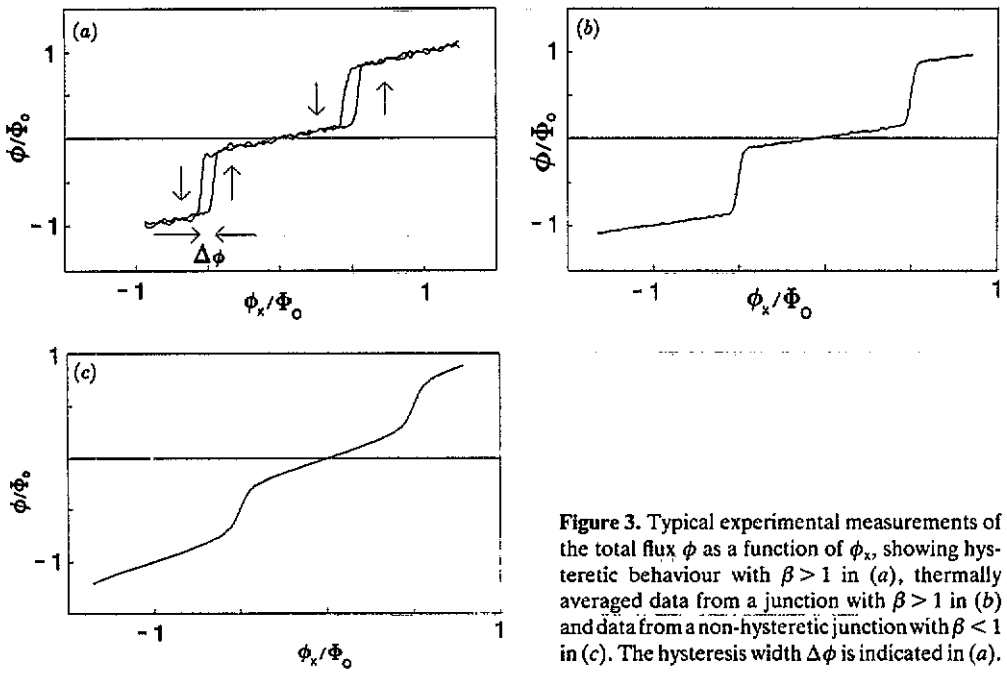

Figure 3. Typical experimental measurements of the total flux ϕ as a function of ϕ_x, showing hysteretic behaviour with $\beta > 1$ in (*a*), thermally averaged data from a junction with $\beta > 1$ in (*b*) and data from a non-hysteretic junction with $\beta < 1$ in (*c*). The hysteresis width $\Delta\phi$ is indicated in (*a*).

Measurements of the magnetization curves of the weak-link structure were made by sweeping a current through the coil in one hole of the device and recording the flux in the other hole using the external SQUID magnetometer. In this way, a plot of the applied flux against the internal flux was recorded. At each fixed temperature, up to 200 sweeps were made and the measurements were signal averaged. The magnetization curves included contributions from direct magnetic coupling between the holes, which could be determined by closing the central link to make a strong superconducting contact (i.e. one where $\beta \rightarrow \infty$). This background slope was then subtracted from all the other data before it was processed as described below. Typical results are shown in figure 3.

Direct measurements of the current–voltage characteristics were made with the outer links open. These were made before and after recording a set of magnetization curves (with the links closed) for a particular setting of the junction. Only when these two current–voltage characteristics were essentially identical could we be sure that the mechanical adjustment of the outer screws had not affected the central junction.

An absolute measurement of the SQUID inductance, L, was made by injecting a current into the tip of the point contact through two thin strips of conductor, separated by a thin insulator, which were trapped between the central point and the flat anvil. The inductance was determined by measuring the flux in the weak-link structure as a function of the current applied to the point. An absolute calibration of the flux measurements was made by subsequently screwing the point down so that it pierced the electrodes to form a weak link yielding magnetization curves periodic in the flux quantum. The resulting value of the inductance is $(6.58 \pm 0.07) \times 10^{-10}$ H, which is consistent with estimates based on the geometry of the device. It should be emphasized that this method directly determines the inductance actually in parallel with the junction (i.e. that of the two holes in parallel modified by the contribution from the structure in the immediate

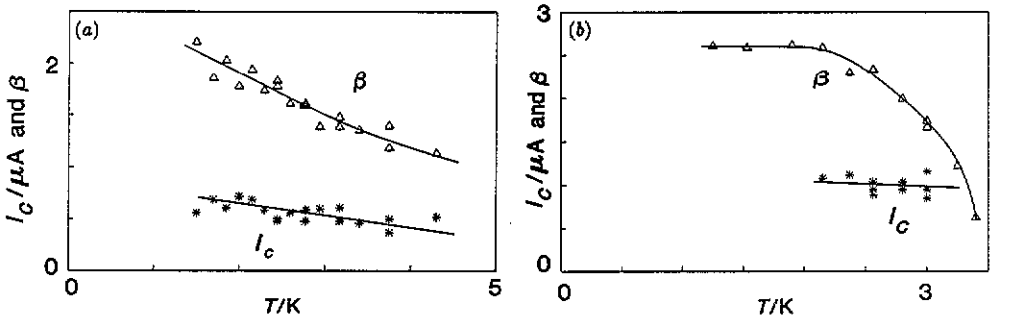

Figure 4. The parameter β for two junctions as measured from the slope of the ϕ against ϕ_x curve at the origin. For the same junctions I_c was derived from fitting the thermally averaged $\langle\phi\rangle$ against ϕ_x assuming the relations in equations (6) and (7). Both quantities are shown as functions of temperature.

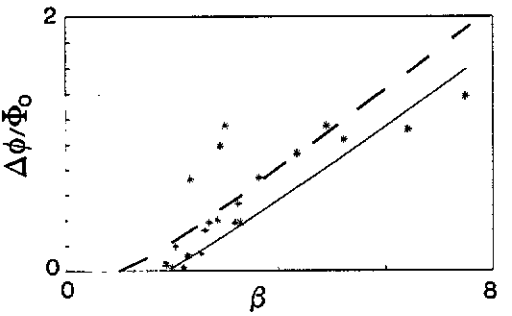

Figure 5. The hysteresis width $\Delta\phi$ (cf figure 3) plotted against the parameter β for a number of hysteretic junctions at 1.25 K. The lines represent the theoretical predictions assuming a sinusoidal current–phase relationship with the experimental temperature (full curve) and $T = 0$ (broken curve), respectively.

vicinity of the point) and that this is exactly the inductance L that appears in the weak-link theory discussed earlier.

4. Results and comparison with theory

Measurements of several hysteretic and non-hysteretic magnetization curves were made on a number of junctions. In the non-hysteretic case, the results were fitted to the thermally averaged sinusoidal junction model described by equations (6) and (7), and the resulting temperature dependences of β and I_c for two of the junctions are shown in figure 4. The relationship $\beta = (2\pi L/\Phi_0)I_c$ is reasonably consistent with the data shown in figure 4(a), but in figure 4(b) the experimentally measured quantities clearly have quite different temperature dependences, indicating a clear discrepancy between the measurements and the model. Moreover, the implied values of the inductance are temperature dependent and only approximately equal to the measured inductance, which was measured to be independent of temperature as expected.

Hysteretic magnetization curves at 1.25 K were recorded for a number of junctions and a value of β obtained in each case from the slope at the origin. The hysteresis width defined as the distance between the mean jumping positions indicated in figure 1(a) was also measured and the results are plotted in figure 5. This figure also shows the maximum width allowed by the theory described above (assuming the experimentally measured

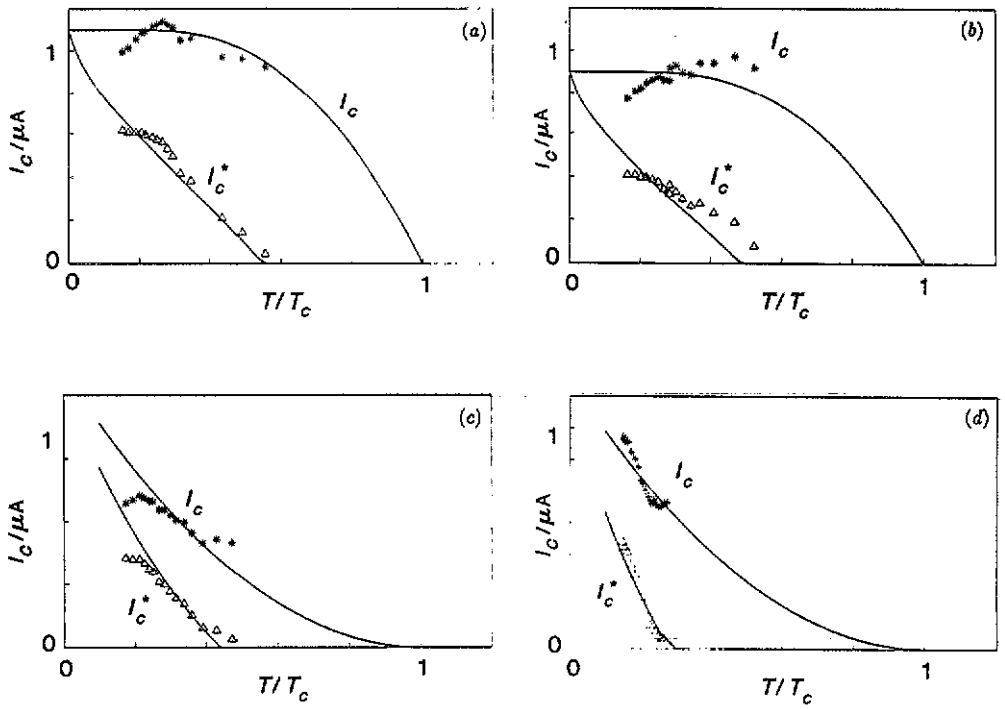

Figure 6. The critical currents for a number of junctions measured with the outer links open. The currents required to produce a voltage of 1 μV are indicated by I_c^* and the critical currents derived from I_c^* by correcting for thermal excitation are indicated by I_c. The full curves represent possible fits to the theoretical forms for SIS junctions (a, b) and SNS junctions (b, c).

value of L), which is what should be observed at $T = 0$ in the absence of MQT, and the width predicted at $T = 1.25$ K assuming that the thermal activation is in line with the theory of Kurkijarvi [10]. If this model is correct, the experimental points should lie on the $T = 1.25$ K line. However, the results indicate that for several junctions the hysteresis width is significantly larger than that expected from the theory, and for some the flux jumps occur in the region above the $t = 0$ line, which is clearly unphysical in terms of the theory developed so far. Once again we have a marked discrepancy between experiment and theory.

We now turn to the critical-current measurements made by recording current–voltage characteristics with the outer links open. Figure 6 shows the measured values of $I_c(T)^*$ (defined as the minimum current required to generate 1 μV across the junction) for four different junctions and the corresponding values for $I_c(T)$ obtained using equation (8). The results shown in figure 6(a) and (6b) have a temperature dependence approximately consistent with the Ambegaokar and Baratoff [9] form for a superconductor–insulator–superconductor (SIS) Josephson junction, while those shown in figures 6(c) and 6(d) are more consistent with that expected for superconductor–normal metal–superconductor (SNS) junctions.

A comparison between the corrected $I_c(T)$ critical-current measurements taken from the current–voltage characteristics and those obtained from magnetization curves on

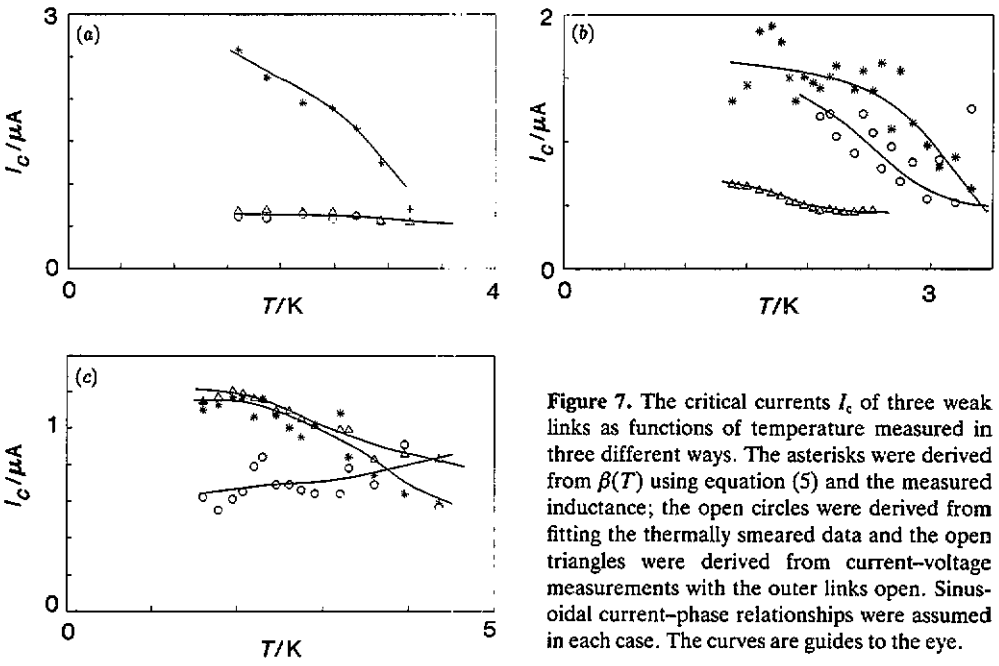

Figure 7. The critical currents I_c of three weak links as functions of temperature measured in three different ways. The asterisks were derived from $\beta(T)$ using equation (5) and the measured inductance; the open circles were derived from fitting the thermally smeared data and the open triangles were derived from current–voltage measurements with the outer links open. Sinusoidal current–phase relationships were assumed in each case. The curves are guides to the eye.

the same junction have been made for several adjustments of the inner link. Values for I_c were also obtained from β by substituting the measured inductance of the SQUID into equation (5). Altogether, therefore, we have three independent determinations of the temperature dependence of I_c as shown in figures 7(*a–c*). It is clear that significant discrepancies occur between the three determinations of I_c for the data represented here.

We therefore conclude that the model of the weak-link ring described by equations (6) and (7) is inadequate to describe the observed properties of our niobium point contact weak-link structure. Moreover, MQT cannot account for the observed discrepancies. For the hysteretic magnetization measurements, MQT would reduce the hysteresis width below that expected from thermal activation because the tunnelling probability would be enhanced at low temperatures causing early flux transitions, while our measurements (figure 4) indicate hysteresis widths that are larger than expected. For the non-hysteretic magnetization measurements, MQT processes could result in a discrepancy between the temperature dependence of β and I_c at low temperature, but not the large discrepancies observed at all temperatures.

A probable explanation for the observed failure of the model to account for our measurements is the possibility of a non-sinusoidal current–phase (*I–S*) relationship in the Josephson weak link. Several authors have suggested that niobium point contacts may be non-sinusoidal [13] for large critical currents, although it has generally been assumed that junctions with critical currents in the range used in this experiment are effectively sinusoidal [3].

A direct measurement of the current–phase relationship can be made only on weak-link structures with $\beta < 1$, where the phase S across the junction is proportional to the single-valued flux ϕ through the loop [14], as illustrated theoretically in figure 1(*b*) and experimentally in figure 3(*c*). The thermally averaged current through the junction is

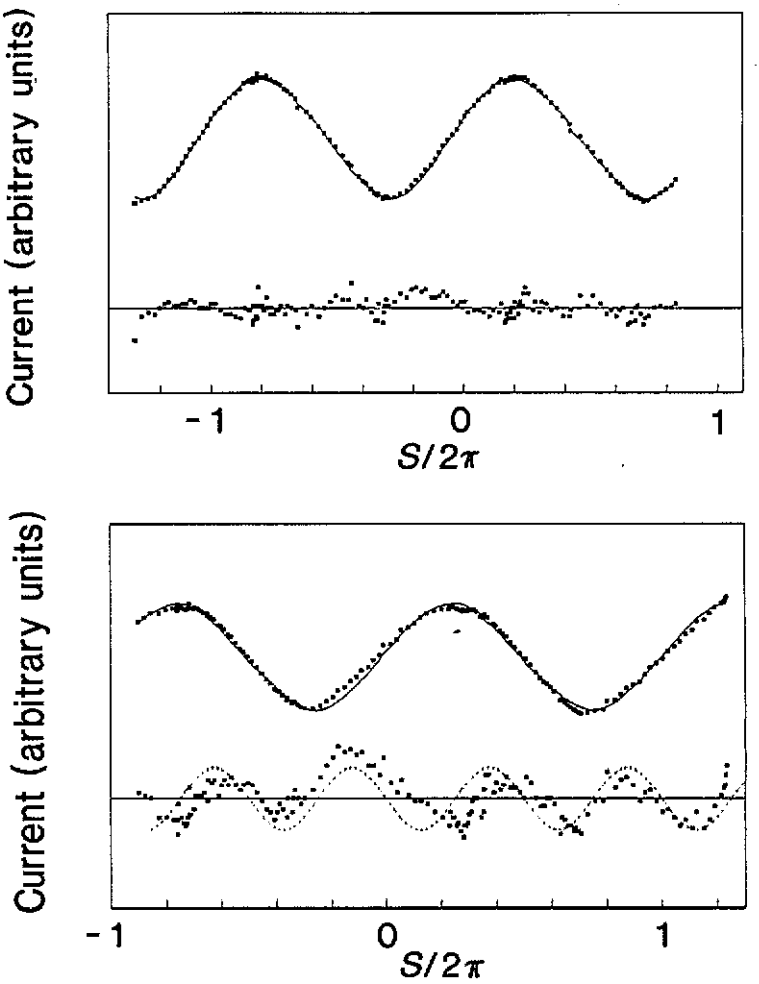

Figure 8. The current–phase relationships measured for two non-hysteretic ($\beta < 1$) weak links. The upper sets of points indicate measured values of $\phi_x - \langle\phi\rangle$ against $\langle\phi\rangle/\Phi_0$, and the curves passing close to them represent the best fits assuming a thermally averaged sinusoidal current–phase relationship. The lower sets of points represent five times the difference between these experimental and fitted values and the broken curve in (*b*) corresponds to a second-harmonic correction.

proportional to the difference between ϕ_x and $\langle\phi\rangle$. Therefore, by obtaining magnetization curves in the case were $\beta < 1$, and plotting $\phi_x - \langle\phi\rangle$ against $\langle\phi\rangle$, the form of the thermally smeared *I–S* relationship may be observed.

Measurements of non-hysteretic magnetization curves were made for several adjustments of the centre link with $\beta < 1$ in each case, implying extremely weak junctions with $I_c < 0.5\ \mu A$. The curves were fitted against the sinusoidal model (cf equation (6)) as before and plotted in the manner described above (figure 8). It is important to note that the theoretical curve includes the influence of thermal activation and is consequently different from a simple sine curve. Significant discrepancies were observed in some cases and figure 8 shows examples of a very nearly sinusoidal and a significantly non-sinusoidal

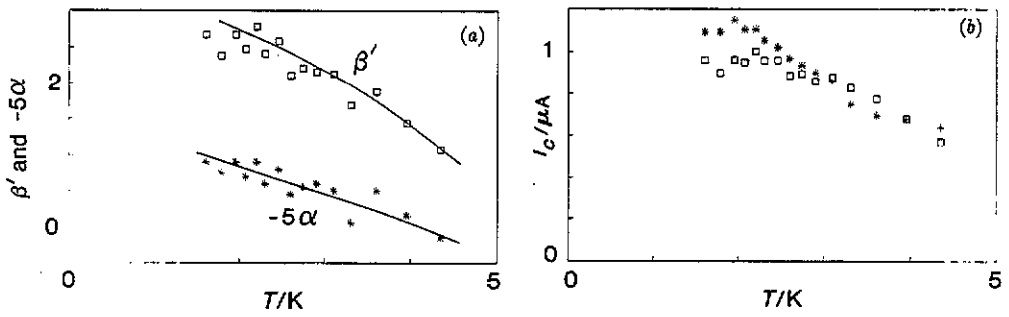

Figure 9. (*a*) The parameters β' and α as functions of temperature for a junction, assuming a thermally averaged model with a second-harmonic contribution to the current–phase relationship. Part (*b*) shows the critical current obtained in the same way (open squares) and that derived from current–voltage measurements (asterisks).

I–S relationship. The differences between experiment and theory are shown; in figure 8(*b*) it is clear that they could be reasonably represented by a comparatively small second-harmonic term.

5. Non-sinusoidal current–phase relationships

As non-sinusoidal behaviour has been observed in our weakest junctions, it is likely to be significant for all of them; we have therefore developed a theory for the weak-link structure that includes a second-harmonic term in the *I–S* relationship. A modified Josephson relationship to include a second-harmonic term may be written as

$$I = I_0[(1 - 2\alpha)\sin S + \alpha \sin(2S)] \tag{9}$$

where this form is chosen to ensure that the slope of the current–phase relationship at the origin is independent of α. The critical current, I_c, obtained by differentiating (9) with respect to S is now

$$I_c = I_0(1 - C^2)^{1/2}(1 - 2\alpha + 2\alpha C) \tag{10}$$

where

$$C = \cos S = [2\alpha - 1 + (1 - 4\alpha + 36\alpha^2)^{1/2}]/8\alpha. \tag{11}$$

The corresponding magnetization curve is given by

$$\phi_x = \phi + LI_0[(1 - 2\alpha)\sin(2\pi\phi/\Phi_0) + \alpha \sin(4\pi\phi/\Phi_0)]. \tag{12}$$

The energy of the weak-link ring may now be expressed as

$$E(\phi, \phi_x) = I_0 \left\{ \frac{\pi}{\phi_0} \frac{(\phi - \phi_x)^2}{\beta'} - \left(\frac{\phi_0}{2\pi}\right)\left[(1 - 2\alpha)\cos\left(\frac{2\pi\phi}{\Phi_0}\right) + \frac{\alpha}{2}\cos\left(\frac{4\pi\phi}{\Phi_0}\right)\right]\right\} \tag{13}$$

where

$$\beta' = 2\pi LI_0/\Phi_0 \tag{14}$$

and the slope of the magnetization curve at the origin is now $1/(1 + \beta')$. The fitting

program for the magnetization curves was modified to work with this new form for the device energy. The analysis of the current–voltage measurements also requires modifiction to include the second-harmonic effects. It is a straightforward extension of the procedure derived by Keene [8] to show that equations (9) and (10) still hold with U_0 replaced by U_0' where

$$U_0' = 0.3I_c\Phi_0(1 - 2\alpha + 2\alpha C)^{1/2}/(1 - 2\alpha + 8\alpha C)^{1/2}. \tag{15}$$

Returning now to the two sets of current–phase data derived from reversible ($\beta < 1$) magnetization curves and shown in figure 8, we adapted the fitting routine to include the additional parameter, α, and now held the inductance, L, at its independently measured value. In the first case the second-harmonic term is negligibly small ($I_0 = 0.97\,\mu$A, $\alpha = 0.00$) but in the second it is significant ($I_0 = 0.64\,\mu$A, $\alpha = -0.09$) and the second-harmonic contribution in this case is shown in figure 8(b) where it is seen to be in good agreement with the experimental data. Substituting the above values in (10) and (11) yields a value of $0.76\,\mu$A for the critical current, about 20% higher than the value obtained when the second-harmonic correction is ignored.

We believe that all the discrepancies in our earlier data can be attributed to the assumption of a sinusoidal current–phase relationship. Reconsidering first the hysteretic data summarized in figure 5 we see that the hysteresis widths $\Delta\phi$ are nearly all somewhat higher than predicted using [5] and the value of β obtained from the slope of the curve of ϕ against ϕ_x at the origin. This is consistent with the value of the critical current being higher than predicted by the model. As we have seen above the addition of a second-harmonic contribution with a negative value for α will lead to just such an increase in critical current with the same slope at the origin. Clearly the discrepancies in the hysteretic data can all be resolved in this way, although we note that there is no independent check on the correctness of the procedure. The same is true for the non-hysteretic data shown in figure 4; in the presence of a second-harmonic correction β becomes β' [14] and is no longer in a one-to-one correspondence with the critical current.

An independent check should be possible in the cases where the critical currents have been derived from the current–voltage measurements made with the outer links open as well as from non-hysteretic magnetization curves (figure 7). We attempted to fit this magnetization data to the new model holding the ring inductance at its measured value and refining the values of I_c and α. It turned out that these parameters were strongly correlated in the least-squares refinement and only the data illustrated in figure 3(c) were of sufficient quality for this procedure to be successful. The resulting temperature dependence of β' and α in this case are shown in figure 9(a) where they are seen to be smoothly varying functions of temperature. The current–voltage measurements were also reanalysed using the new model to obtain values for I_c. These results are also shown in figure 9(b) where we see that the previous discrepancies have been resolved and there is now good agreement between these independent determinations of I_c.

We have therefore demonstrated that magnetization curves for our niobium point contact weak-link structures can be successfully fitted to a model that includes a second-harmonic contribution to the I–S relationship in the Josephson junction. It was not found necessary to include a contribution from MQT in order to fit our data to the otherwise thermally activated model for the SQUID. The values for $I_c(T)$ that were obtained from the independent electrical measurements on the isolated Josephson junction were found to be consistent with those found from magnetic measurements on the SQUID.

6. Discussion

We have found that for nearly all the point contacts we have studied, the current–phase relationship is significantly non-sinusoidal, although generally good fits can be obtained if a single extra parameter representing a second-harmonics term is included. Such second-harmonic terms are generally believed to be associated with tunnelling events in which more than one pair tunnels at a time and are therefore expected to be comparatively less important for small critical-current junctions. The fact that we have seen evidence for second-harmonic contributions in the case of very weak junctions may be associated with our small-area point contacts and the relatively high current densities associated with them. Given the non-sinusoidal properties of our junctions and the temperature dependence of the critical currents, we have been able to explain all our results using models based on thermal activation and have found no evidence for significant quantum effects. This is consistent with our expectation that quantum effects should be negligible for such devices in this temperature range if the electromagnetic properties of the whole SQUID structure and not just the point are allowed for.

Some of the conclusions from previous work may well also be affected by their neglect of possible non-sinusoidal current–phase relationships. In particular, the results reported in [2] and [3] use critical currents derived from values of β obtained from the slopes of the magnetization curves near the origin. As pointed out above, quite small second-harmonic terms can significantly affect the relationship between the critical current (and hence the hysteresis width) and this slope and the evidence for quantum effects in this work is therefore inconclusive. The measurements on fabricated structures [4, 5] also assume sinusoidal current–phase relationships, but they are less likely to be seriously affected as the measurements are made with the devices biased very close to I_c. However, it is possible that the small discrepancies between theory and experiment noted in [4] may be attributable to non-sinusoidality.

Finally, we refer to the results of the Sussex group [1]. Their measurements are consistent with a quantum model given a very small capacitance similar to that expected from the point contact alone and a very small value of the dissipation. Moreover, their results appear to suggest not only the existence of quantum tunnelling but also of quantum coherence, which should be even more difficult to observe. These results cannot be reconciled to a classical model simply by the inclusion of a non-sinusoidal current–phase relationship. A fundamental inconsistency therefore remains between their results and the predictions of standard quantum theory including the effects of the electromagnetic environment.

Acknowledgments

We re very grateful to Mr G Walsh who built the apparatus and without whose technical expertise the experiments would have been impossible. We thank the UK Science and Engineering Research Council and the National Physical Laboratory for support for one of us (MNK).

References

[1] Prance R J, Multon J E, Prance H, Clark T D, Widom A and Megaloudis G 1983 *Helv. Phys. Acta* **56** 789–95

Mutton J E, Prance R J and Clark T D 1984 *Phys. Lett.* **104A** 375
[2] den Boer W and de Bruyn Ouboter R 1980 *Physica* B **89** 185–90
[3] de Bruyn Ouboter R 1984 *Physica* B **126** 423–30
[4] Schwartz D B, Sen B, Archie C N and Lukens J E 1985 *Phys. Rev. Lett.* **55** 1547–9
[5] Sharifi F, Garilano J L and Van Harlingen D J 1988 *Phys. Rev. Lett.* **61** 742–5
[6] Rae A I M and Gough C E 1986 *J. Low Temp. Phys.* **65** 283–6
[7] Devoret M H, Esteve D, Grabert H, Ingold G-L, Pothier H and Urbina C 1990 *Phys. Rev. Lett.* **64** 1824–7
[8] Keene M N 1990 *Supercond. Sci. Technol.* **3** 312–14
[9] Ambegaokar V and Baratoff A 1963 *Phys. Rev. Lett.* **11** 104
[10] Kurkijarvi J 1972 *Phys. Rev.* B **6** 832–5
[11] Ivanchenko Y M and Zil'berman L A 1968 *JETP Lett.* **8** 113–15
[12] Ambegaokar V and Halperin B I 1969 *Phys. Rev. Lett.* **22** 1364–6
[13] Jackel L D and Bohrman R A 1975 *J. Low Temp. Phys.* **19** 201–246
[14] Waldram J R and Lumley J M 1975 *Rev. Phys. Appl.* **10** 7–10